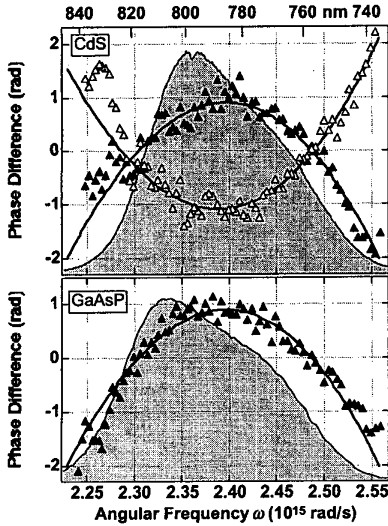

CWA49 Fig. 3. TPA experiments: Optimum phase minus reference phase for the photoluminescence experiment on the CdS thin film and the photocurrent experiment on the GaAsP photodiode. Full triangles: (phase for +207 fs^2 bias GDD)—(reference phase). Open triangles: (phase for –207 fs^2 bias GDD)—(reference phase). The solid lines have been calculated, see text. Grey: power spectra of the laser pulses.

using the TPA data of Figs. 1 and 2. This experimental difference phases is compared to the phase difference that can be calculated from the known settings of the 4-prism sequence,[6] see Fig. 3. The good agreement shows that TPA-based adaptive pulse compression can accurately compensate for phase distortions introduced by dispersive optical elements. This result reconfirms that reliable compression to the bandwidth limit can be achieved with this approach.

References

*) Present and permanent address: CSEM, CH-6055 Alpnach, Switzerland.

1. D. Meshulach and Y. Silberberg, "Coherent quantum control of two-photon transitions by a femtosecond laser pulse," *Nature (London)* 396, 239 (1998).
2. N. Dudovich, B. Dayan, S.M. Gallagher Faeder, and Y. Silberberg, "Transform-limited pulses are not optimal for resonant multiphoton transitions," *Phys. Rev. Lett.* **86**, 47 (2001).
3. D. Meshulach, D. Yelin, and Y. Silberberg, "Adaptive ultrashort pulse compression and shaping," *Opt. Commun.* 138, 345 (1997).
4. T. Brixner, M. Strehle, and G. Gerber, "Feedback-controlled optimization of amplified femtosecond pulses," *Appl. Phys. B* **68**, 281 (1999).
5. J. Kunde, B. Baumann, S. Arlt, F. Morier-Genoud, U. Siegner, and U. Keller, "Optimization of adaptive feedback control for ultrafast semiconductor spectroscopy," *J. Opt. Soc. Am. B* 18, 872 (2001).
6. R.L. Fork, O.E. Martinez, and J.P. Gordon, "Negative dispersion using pairs of prisms," *Opt. Lett.* 9, 150 (1984).

CWA50 **1:00 pm**

Nonlinear Behaviors of LTG-GaAs Based MSM TWPDs Under Telecommunication Wavelength Excitation

Jin-Wei Shi, Graduate Institute of Electro-Optical Engineering, National Taiwan University, Taipei 10617, Taiwan, Email: bd0122@ms17.hinet.net

Kian-Giap Gan, Department of Electrical and Computer Engineering, University of California, Santa Barbara, CA 93106

Yen-Hung Chen, Graduate Institute of Electro-Optical Engineering, National Taiwan University, Taipei 10617, Taiwan

Yi-Jen Chiu, and John. E. Bowers, Department of Electrical and Computer Engineering, University of California, Santa Barbara, CA 93106

Chi-Kuang Sun, Graduate Institute of Electro-Optical Engineering, National Taiwan University, Taipei 10617, Taiwan

Recently, the development of optical amplifier has created a new demand for high available power in ultra-high speed photodetectors. However, these ultrahigh bandwidth photodetectors usually suffer bandwidth degradation problems under intense optical power illumination.[1] Low-temperature-grown-GaAs (LTG-GaAs) based photodetector is the most attractive one among the ultrahigh speed photodetectors with high available output power.[2] Recently, record-high power-bandwidth-product performances of LTG-GaAs-based metal-semiconductor-metal traveling-wave-photodetector (MSM TWPD)[3] in short (~800 nm) and long wavelength (~1300 nm) regimes both have been demonstrated[4,5] due to short carrier trapping time of LTG-GaAs in both wavelengths and its superior microwave guiding structure.

The observed nonlinear saturation behaviors of LTG-GaAs MSM TWPD under long (~1300 nm) and short (~800 nm) wavelength excitation are very different. MSM TWPD structures at these two operating wavelengths are the same and are given in,[3] except that the device absorption lengths in long and short wavelength regime are 70 μm and 10 μm respectively due to different modal absorption constants. We employed Cr^{4+}: forsterite and Ti:sapphire lasers operating at 1230 nm and 800 nm as the light sources for the transient electro-optical (EO) sampling measurements. Figure 1(a) and 1(b) includes the measured normalized E-O sampling traces A~D for different optical pumping energy at a fix bias voltage (15 V) under short and long wavelength excitations with almost the same amount of collected photo-generated carriers. The required optical pumping energy in figure 1(a) is lower than 1(b) due to much larger absorption coefficient at short wavelength. In figure 1(a), with a much shorter absorption length and higher photo-generated carrier density than in the case of figure 1(b), there was no obvious broadening in the measured E-O traces even with the highest pumping power (trace D). However, the results at long wavelength as shown in the traces of A~D in figure 1(b) showed a much serious broadening with increased pumping power. Because of the much lower generated carrier density ($\sim 2 \times 10^{17}$ cm^{-3}) in trace D under long wavelength excitation than the defect density in LTG-GaAs layer ($\sim 1 \times 10^{18} cm^{-3}$) and because of the behaviors of non-broadening under short wavelength excitation with much higher density of photo-generated carriers, we can attribute these saturation behav-

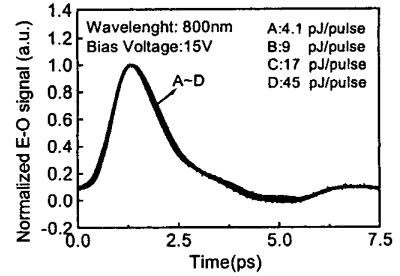

Figure 1(a)

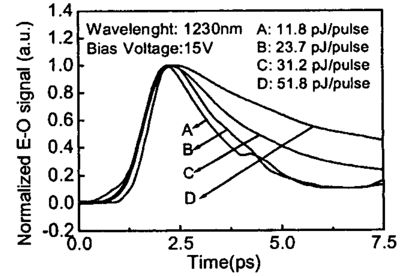

Figure 1(b)

CWA50 Fig. 1. Measured normalized E-O sampling traces (a) under short wavelength (800 nm) and (b) long wavelength excitation at a fix bias voltage and different optical pumping energy with the same amount of collected photo-generated charge. The decay time constant of traces A~D in (b) is 1.48 ps, 1.76 ps, 2.92 ps, and 5.7 ps.

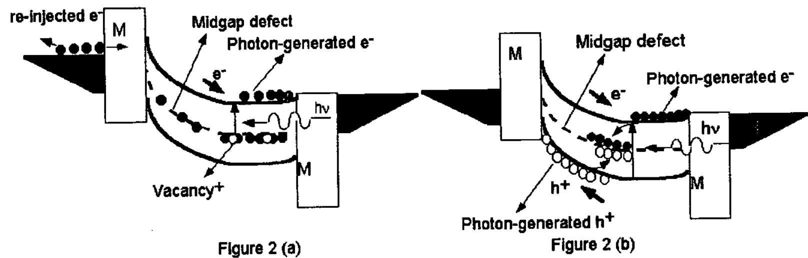

CWA50 Fig. 2. Conceptual band diagram of LTG-GaAs under (a) long wavelength and (b) short wavelength excitation.

iors to different carrier transport dynamics under these two different excitation mechanisms.

The dominant absorption processes of LTG-GaAs under long wavelength excitation is the transition from mid-gap defect states to conduction band as shown in figure 2(a). The dominant transport carrier type is electron. Some immobile vacancies also existed in the mid-gap defect states of LTG-GaAs photo-absorption layer after excitation. In order to support charge neutrality, electrons must be re-injected from negative electrode to neutralize these leftover vacancies. The dominant absorption processes of LTG-GaAs under short wavelength excitation is the transition from valence band to conduction band as shown in figure 2(b). Electron and hole are both the dominant transport carrier types. Charge neutralization can be supported by electron-hole recombination. We believe that the distinct nonlinear saturation behaviors observed are thus related to these two distinct carrier transport dynamics. More detailed experiments and simulation results will be given in the conference.

References

1. K. Kato, *IEEE Trans. On Microwave Theory Tech.*, vol. 47, pp. 1265–1281, Jul. 1999.
2. Y.J. Chiu, *et al., Conference on Lasers and Electro-Optics*, OSA Technical Digest, pp. 501–502, May, 1998.
3. J.-W. Shi, *et al., IEEE Photon. Techno. Letters*, vol. 16, pp. 623–625, June, 2001.
4. J.W. Shi, *et al.*, to be published in Conference Proceeding of *IEEE Lasers and Electro-Optics Society 2001 Annual Meeting.*
5. J.-W. Shi, *et al.*, to be published in *IEEE Photon. Techno. Letters.*

CWA51 1:00 pm

Probing Voltage Waveforms in Semiconductor Devices Using Electric Field Induced Second Harmonic Generation

Daniel J. Kane and Kristen A. Peterson, Southwest Sciences, Inc. 1570 Pacheco St., Suite E-11, Santa Fe, NM 87505, Email: djkane@swsciences.com

1. Introduction

Evaluation of fast semiconductor devices requires both high temporal resolution and the ability to probe internal points of an IC noninvasively. While optical methods are suitable for this application, centrosymmetric semiconductors such as silicon and germanium require an external electro-optic probe placed within the fringe electric field flux lines of the region of interest, reducing sensitivity and adding parasitic capacitance to the probed circuit. In this work, we apply Electric Field Induced Second Harmonic Generation (EFISHG) to the measurement of voltage waveforms in the active region of GaN semiconductor devices without the use of any external electro-optic probe.

While voltages in semiconductors are quite small, because the voltage drop occurs only over a very narrow depletion region, electric fields can surpass 10^6 V/cm. Such large electric fields can interact with an external probe laser via the $\chi^{(3)}$ of the semiconductor producing second harmonic of the probe laser ($P \propto \chi^{(3)} E_{DC} E_{probe}^2$). Generally a weak effect, the large electric fields present in semiconductors, together with the large $\chi^{(3)}$'s of semiconductors, make this effect observable.

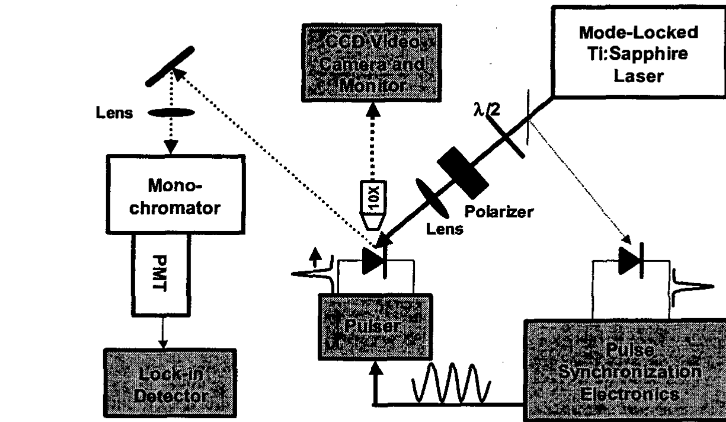

CWA51 **Fig. 1.** Schematic of apparatus for waveform measurement using electric field induced second harmonic generation.

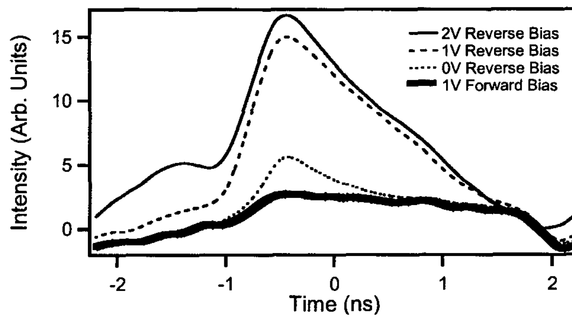

CWA51 **Fig. 2.** Measured voltage waveform across the active region of a GaN UV LED at four different bias voltages.

2. Experimental

Figure 1 shows a schematic of the apparatus used for electric field induced second harmonic generation. The probe laser beam at the fundamental wavelength is focused onto a semiconductor sample (in this case a UV light emitting diode (LED)) to a spot size of ~20 μm. A half-wave plate and polarizer are used for variable attenuation and polarization control of the probe beam. The probe beam is incident at 45 degrees to the sample surface. The reflected signal is directed though a 1/4 meter spectrometer. UV pass/visible blocking filters are used in front of the spectrometer to block any residual fundamental before reaching the 1P28 photomultiplier tube (PMT). The electronic pulses in the LED and the ultrashort laser pulses (<100 fs) from the mode-locked Ti:sapphire laser are synchronized and time delayed using custom synchronization electronics. (806 nm fundamental is used to insure both the fundamental and second harmonic is below the bandgap of the probed material in order to reduce induced photocurrents.) A microscope objective above the sample and a CCD camera are used to visualize the alignment of the probe beam on the diode. A pico-ammeter (not shown) can be used to monitor photo-induced current.

3. Results

Figure 2 shows the electronic pulse measured across the p-n junction as a function of junction bias voltage (DC). As the junction becomes more forward biased, the diffusion capacitance increases, reducing the voltage drop of the high-speed pulse (<1 ns). The EFISHG signal due to the applied voltage is heterodyned with a background EFISHG signal caused by the piezoelectric fields present in GaN. As a result, the measured EFISHG signal appears linear in applied voltage.

These results demonstrate it is possible to monitor an electric field within the device using EFISHG. Additional results, showing the SHG spectrum, probe laser wavelength dependence, and waveform tracking will also be presented. Ultimately, we hope to use this technique to probe silicon-based integrated circuits using infrared light.

Reference

1. K.A. Peterson and D.J. Kane, Opt. Lett. 26, 438–440 (2001).